Volume 3 | Number 40 | 28 October 2015 | Pages 10319–10652

Journal of Materials Chemistry C

Materials for optical, magnetic and electronic devices

www.rsc.org/MaterialsC

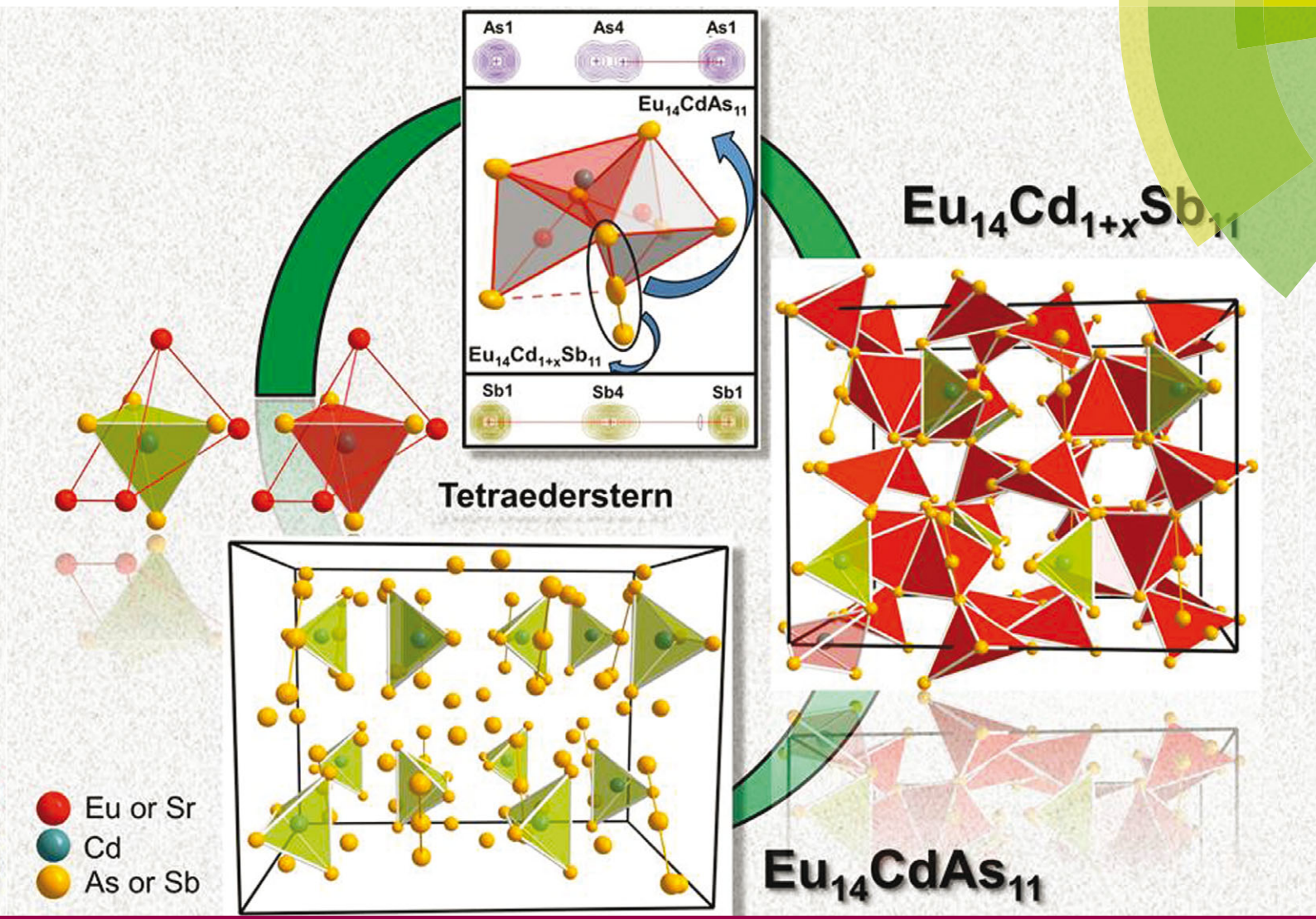

Themed issue: Thermoelectrics

ISSN 2050-7526

ROYAL SOCIETY OF CHEMISTRY

PAPER

Svilen Bobev *et al.*

Non-stoichiometric compositions arising from synergistic electronic and size effects. Synthesis, crystal chemistry and electronic properties of $A_{14}Cd_{1+x}Pn_{11}$ compounds ($0 \le x \le 0.3$; A = Sr, Eu; Pn = As, Sb)

Journal of
Materials Chemistry C

PAPER

View Article Online
View Journal | View Issue

Cite this: *J. Mater. Chem. C*, 2015, 3, 10388

Non-stoichiometric compositions arising from synergistic electronic and size effects. Synthesis, crystal chemistry and electronic properties of $A_{14}Cd_{1+x}Pn_{11}$ compounds ($0 \leq x \leq 0.3$; A = Sr, Eu; Pn = As, Sb)†

Julien P. A. Makongo, Gregory M. Darone, Sheng-Qing Xia and Svilen Bobev*

Received 2nd June 2015,
Accepted 9th July 2015

DOI: 10.1039/c5tc01605c

www.rsc.org/MaterialsC

The structural variability in terms of existence of stoichiometric and nonstoichiometric compounds in the well-known "14–1–11" family has been investigated. Four such compounds, $Eu_{14}CdAs_{11}$, $Sr_{14}Cd_{1.06(1)}As_{11}$, $Eu_{14}Cd_{1.27(1)}Sb_{11}$, and $Sr_{14}Cd_{1.30(1)}Sb_{11}$, synthesized by both flux and traditional solid-state methods, have been structurally characterized by single-crystal X-ray diffraction. They are all isotypic, forming with the $Ca_{14}AlSb_{11}$ structure type (Pearson code *tI*208, tetragonal space group $I4_1/acd$). Their average structure can be described as space-filling packing of distorted [APn_6] octahedra, [APn_5] trigonal bipyramids, and [$CdPn_4$] tetrahedra, where Pn denotes As or Sb, and A stands for Eu or Sr. Interstitial sites are partially occupied by Cd atoms, giving rise to the chemical formula $A_{14}Cd_{1+x}Pn_{11}$. The interstitial atom can be seen as forming a cluster, reminiscent of the empty substructure unit in the gamma-brass cluster (also known as "tetraederstern"). Robust cation–cation interactions exist in the structure and might be a natural response of the electronic structure to compensate for the apparent electron deficiency and in order to optimize the bonding interactions. The electronic structure calculations for idealized $Sr_{14}CdSb_{11}$ revealed that the Fermi level falls near the edge of the valence band, which suggests poor metallic conductivity. The analysis of the volume of coordination polyhedron and that of the Voronoi cell indicates that the content of Cd atoms in the interstitial site is limited by the available "free volume" within the complex tetrahedral unit. This free volume is induced by the instability of the hypervalent $[Pn_3]^{7-}$ anion, which in turn is related to the increasing size of pnictogen atoms, and to some extent, by the type/size of the countercations.

1 Introduction

The recent discovery of interesting magnetic, electronic and thermal transport properties in the family of tetragonal Zintl compounds $A_{14}MPn_{11}$ (where A stands for the divalent electropositive metals Ca, Sr, Ba, Eu, or Yb, M is one of the triel elements Al, Ga, In or transition metal such as Mn, and Pn = pnictogen, *i.e.*, P, As, Sb, Bi) has sparked considerable interest in this class of materials. Not only do these compounds provide a basis for understanding the structural flexibility as a function of the size of the pnictogen atoms, the electropositive A metal, and the M metal atoms, but they also represent a unique class of materials having the ability to integrate, in a single class of compounds, a wide variety of physical properties including ferromagnetic or antiferromagnetic ordering, colossal magnetoresistance, as well as (semi)metallic and semiconducting properties with direct implication for high temperature thermoelectric power generation.[1] This profusion of unusual physics can be ascribed to the complex crystal structure of these compounds, which adopt the $Ca_{14}AlSb_{11}$ structure type.[2] In terms of the Zintl–Klemm concept,[1a,3] the $Ca_{14}AlSb_{11}$ structure can be rationalized as consisting of 14 Ca^{2+} cations and three types of anions—the $[AlSb_4]^{9-}$ tetrahedral species, isolated $[Sb]^{3-}$, and the linear hypervalent $[Sb_3]^{7-}$. The latter seems to be the hallmark of the structure, impacting strongly the bonding and the properties of these compounds. Surveying the literature, we have noticed that not all linear $[Pn_3]^{7-}$ units are created equal,

Department of Chemistry and Biochemistry, University of Delaware, Newark, Delaware 19716, USA. E-mail: bobev@udel.edu; Fax: +1-302-831-6335; Tel: +1-302-831-8720

† Electronic supplementary information (ESI) available: Crystallographic information files (CIF), crystallographic data for $Sr_{14}Cd_{1.4(1)}Sb_{11}$, obtained *via* a stoichiometric reaction of the elements, relevant plots of the electron density from the refined atomic positions of the hypervalent $[Pn_3]^{7-}$, first coordination sphere of the cations in the "14–1–11" structure, alternative description of the structure of $Ca_9Cd_{4+x}Bi_9$ (data taken from ref. 18). See DOI: 10.1039/c5tc01605c

and the hypervalent description might be an oversimplification, particularly in the case of $[P_3]^{7-}$ and $[As_3]^{7-}$, where crystallographic disorder appears to be prevalent. Take for example the $Ca_{14}GaP_{11}$ structure,[4] where the central atom in the presumed $[P_3]^{7-}$ anion is offset from its equilibrium position, resulting in a splitting with a distance between the split sites of *ca.* 0.8 Å. A similar disorder involving $[As_3]^{7-}$ has been reported for $Sr_{14}MnAs_{11}$[5] and $Sr_{14}GaAs_{11}$,[6] among others, where the split atomic positions are *ca.* 0.7 Å apart. This raises the question about the stability of this electron-rich three-center bonding, which Munzarová and Hoffmann[7] addressed, in part,‡ in their computational work studying the hypervalent $[Pn_3]^{7-}$ anions in $Ca_{14}GaAs_{11}$,[8] $Eu_{14}MnSb_{11}$,[9] $Ca_{14}MnBi_{11}$ and $Ba_{14}MnBi_{11}$.[10] A very recent experimental/DFT paper on $Ca_{14}MgSb_{11}$ and $Yb_{14}MgSb_{11}$ [11] provided yet another look at the bonding in $[Sb_3]^{7-}$. From the literature, one might conclude that the electronic requirements of the hypervalent bonding in $[Pn_3]^{7-}$ are a function of both the type of constituent atoms and the type of counter-cations within the crystal structure. If that is the case, one can then ask the question: if an interplay of atomic sizes and electronegativities does exist, what are the conditions that could make one effect override the other? More than a decade-old study offered a glimpse into this problem, but surprisingly, has not inspired follow-up work—the Kauzlarich group identified $A_{14}MSb_{11+x}$ (A = Ca, Sr; M = Zn, Cd),[12] where the structure is shown to accommodate an additional metal atom, which the early study assigned as Sb. With this paper we provide further insight into the interstitial chemistry of the ''14–1–11'' structure and suggest the formulation $A_{14}M_{1+x}Sb_{11}$ to be a more plausible scenario, from both geometric and electronic arguments (*vide infra*).

Herein, we report the synthesis, and an account on the crystal chemistry and electronic properties of the compounds $Eu_{14}Cd_{1+x}As_{11}$, $Sr_{14}Cd_{1+x}As_{11}$, $Eu_{14}Cd_{1+x}Sb_{11}$, and $Sr_{14}Cd_{1+x}Sb_{11}$, which are referred to hereafter, for simplicity, by their idealized stoichiometric formulae. The structures of these compounds can be viewed as space-filling packing of distorted $[APn_6]$ octahedra and $[APn_5]$ trigonal bipyramids, where Pn = As, Sb; A = Eu, Sr. The extra Cd atoms are embedded within part of the residual space near the center of a tetrahedral unit consisting of an inner $[CdPn_4]$ and an outer $[CdA_4]$ tetrahedron. This polyhedral unit is reminiscent of the empty tetrahedral substructure of the gamma-brass cluster. Each $[CdPn_4]$ tetrahedron shares faces with distorted $[APn_6]$ octahedra and $[APn_5]$ trigonal bipyramids. The description of the structure in terms of such complex polyhedral packing is an important element toward the understanding of the origin of the robust Cd–A bonding, furthering the notion that the ''free volume'' of the interstitial site is related to the electronic instability of the linear hypervalent $[Pn_3]^{7-}$ (Pn = As, Sb) anion. By judiciously choosing the two counter-cations (Eu and Sr) and the two pnictogen atoms (As and Sb), we show using the Voronoi cell volume analysis that the propensity of the structure toward additional atom uptake increases with increasing the size of the pnictogen, and to some extent, with the size of the counter-cations. This allows for the accommodation of a small fraction of electron-donating atoms (*i.e.*, Cd, which can fit into the sparse ''free volume'' within the tetrahedral unit, lending support to the notion that Cd^{2+} will be preferred over the much bigger Sb^{3-}, at the minimum, for geometric reasons).

Our study on ''14–1–11'' phases came into being over the course of our careful exploratory studies of ternary pnictides for potential application as thermoelectric materials. This area of research has been one of the core activities in our research group over the past 10 years, and as a result, a large number of new compounds with unique structures have been synthesized and characterized. Several noteworthy examples include, but are not limited to, Ca_2CdSb_2 and Yb_2CdSb_2,[13] $Ba_{11}Cd_8Bi_{14}$,[14] $Eu_{10}Cd_6Bi_{12}$,[15] $A_{11}Cd_6Sb_{12}$,[16] $A_{21}Cd_4Pn_{18}$,[17] $A_9Cd_{4+x}Pn_9$, and $A_9Zn_{4+x}Pn_9$[18] (A denotes Ca, Sr, Ba, Eu, or Yb; Pn stands for As, Sb, Bi). The two latter examples belong to the ''$A_9M_{4+x}Pn_9$'' (M = Mn, Zn, Cd) family, which is closely related, at the structural level, to the title $A_{14}M_{1+x}Sb_{11}$ compounds. Coincidentally, the ''9–4–9'' phases have also been gaining considerable interest due to the recent reports of interesting electronic and thermal transport properties in $Yb_9Mn_{4.2}Sb_9$ and its Zn-substituted variant.[19]

2 Experimental

2.1 Synthetic procedures

All reagents with stated purity greater than 99.9% of the metal basis were used as purchased (Alfa or Aldrich). Single-crystals of the title compounds were grown from the starting elements. The reagents were loaded in 2 cm^3 alumina crucibles, topped with lead metal as a flux medium, and subsequently sealed in fused silica tubes under a vacuum of 10^{-4} Torr. All sample manipulations (prior and post synthesis) were performed inside an argon-filled glove box with oxygen and moisture levels below 0.1 ppm.

The best heat treatment routes were found to be as follows: (1) $Eu_{14}CdAs_{11}$ samples (10-fold excess of Pb) were slowly heated to 1000 °C at a rate of 100 °C h^{-1}, dwelled at this temperature for 16 h for homogenization, and then cooled successively to 900 °C at a rate of 10 °C h^{-1}, to 750 °C at a rate of 2 °C h^{-1}, and finally to 600 °C at a rate of 50 °C h^{-1}, the temperature at which the sample was centrifuged to separate the molten Pb from the crystals. Multifaceted air-stable crystals were obtained and used for single-crystal structure determination. (2) The $Sr_{14}CdAs_{11}$ samples were heated to 1100 °C in 72 h, the temperature at which a dwelling time of 30 h was necessary for sample homogenization before cooling down to 700 °C over 58 h for centrifugation. Irregular, dark-grey crystals were obtained and found to be air-sensitive; (3) $Sr_{14}CdSb_{11}$ samples were heated

‡ Munzarová and Hoffmann (ref. 7) discuss a subtle but important trend with regard to the isoelectronic X_3 linear systems and the strength of the 3-center 4-electron bonding. They argue that the stability of the X_3 species decreases when moving from right to left in the periodic table, but the group trends in s, p mixing are more complex. For the electron-rich tripnictides, the authors argue that the ability to accommodate a hypervalent electron count is the largest in the middle than at the end of group 15.

to 1100 °C in 4 h, held there for 8 h, cooled to 900 °C in 30 h, where another dwelling step of 32 h was introduced before cooling the sample to 700 °C over 20 h for removal of the molten lead by centrifugation. Powder X-ray diffraction analysis revealed the "14–1–11" phase as the major product with minor, unknown impurity phases.

For the $Eu_{14}CdSb_{11}$ samples, which were found to be air-stable, two different strategies were pursued: (1) single-crystals of $Eu_{14}Cd_{1.27(1)}Sb_{11}$ were grown by a reaction of the reagents in the molar ratio Eu : 27 : Cd : 100 : Sb : 18, with Cd having a dual role of reagent and flux. The sample was subsequently heated to 1100 °C over 8 h, equilibrated at this temperature for 30 h, and finally cooled to 700 °C over 50 h for centrifugation. Powder X-ray diffraction revealed the product to be a mixture of $Eu_9Cd_{4.5}Sb_9$, $Eu_{11}Sb_{10}$, and $Eu_{14}CdSb_{11}$. Bulk material of the same composition was prepared by direct fusion of the reagents in the exact molar ratio (*i.e.*, with a stoichiometric amount of Cd) and at the same temperature. The synthesized material was poorly crystalline. Small single-crystals were identified from a similar reaction of Sr, Cd, and Sb and subjected to crystallographic analysis—the synthetic method apparently does not affect the structure, since the refinements are almost identical (ESI†).

Last, we note that attempts to make more isotypic phases were made, but were unsuccessful. For example, we looked into the possibility to synthesize the Ca-, Yb-, and/or Ba-analogs of the herein presented arsenides and antimonides, but succeeded in making $Yb_{14}CdSb_{11}$, $Ba_{14}CdSb_{11}$, and the solid-solution $(Yb,Ca)_{14}CdSb_{11}$ in limited quantities. The structures of these phases remain to be established from single-crystal X-ray diffraction work.§ The synthetic routes described above did not allow us to make any of possible Zn-analogs, although $Yb_{14}ZnSb_{11}$ is known in the literature.[1f] The recurring products of these experiments were the stable binary $A_{11}Pn_{10}$ phases (A = Ca, Sr, Eu, Yb; and Pn = As, Sb), as well as A_2ZnSb_2 (A = Sr, Eu).[20]

2.2 Crystallography

The powder X-ray diffraction data were recorded on a Rigaku MiniFlex powder diffractometer operating with a filtered Cu Kα radiation (λ = 1.54056 Å) and enclosed inside a nitrogen-filled glove-box. This enables one to work with samples prone to decomposition in ambient air. The JADE 6.5 software package was employed for the phase analysis and identification.

Single-crystals were selected inside the argon-filled glove box and cut in Paratone-N oil to a desired shape and size under an optical microscope, then placed on glass fibers, which were immediately mounted on the goniometer of a Bruker SMART CCD-based diffractometer. An inert atmosphere and constant temperature (200 K) were maintained by flowing a cold nitrogen stream over the crystals. A monochromatized Mo Kα radiation (λ = 0.71073 Å) was used for data collection. Four different batches of ω scans with a scan width of 0.40° and an exposure time of 10 s per frame were collected in the 2θ range up to 60° at four different φ settings. The data collection was processed and monitored employing the Bruker SMART software package.[21] The global unit cell refinements, data reduction and integration were completed using the SAINT program.[22] The intensities of the data sets were merged and sorted for space group determination on the basis of systematic absences using the subprogram XPREP in SHELXTL.[23] Semi-empirical absorption corrections based on symmetrically equivalent reflections were applied to all data using SADABS.[24] The structure was solved by direct methods using SIR-92,[25] and refined against F^2 using SHELXL-97, as implemented in WinGX.[26]

The centrosymmetric space $I4_1/acd$ was uniquely identified based on systematic absences, and the structure solution in this space group, in all cases, yielded all nine atomic positions, known in the archetype $Ca_{14}AlSb_{11}$.[2] Isotropic full-matrix least-squares refinement of this model, with only one Cd position, converged to reasonable (albeit somewhat high) residual values for all 4 structures within just a few refinement cycles. At this stage, almost all thermal parameters had isotropic values in the range of 0.02–0.03 $Å^2 \times 10^{-2}$. Independent refinements of the occupancy factor of each atomic position showed all to be fully occupied (within 5–6σ). Noteworthily, freeing occupancy factors did not lead to improved R_1 values, (which for the Sb-compounds in particular, were about 10%), and the high electron density left in the Fourier map (which was above 20 $e^- Å^{-3}$). The extra density was at reasonable distances to heavy atoms, Sb3, Sr1/Eu1 and Sr4/Eu4 being the closest.

All of the above suggested deficiency in the model. In an attempt to account for this electron density, a provisional partially occupied atom was included; for reasons impacting the valence electron count (*vide infra*), this position was assigned as Cd2 and it was refined with a low occupancy factor (*ca.* 1/10 of full). The improvement of the residuals and the electron density map was noticeable—the result was 30% lower R_1 and wR_2 residuals, while the "extra" electron density dropped by *ca.* 60%. This provided a hint that the "interstitial" site must be intrinsic to the structure, even though the As-compounds show very low occupation at the Cd2 site.

Refinements of the models with the "interstitial" Cd2 included and with anisotropic displacement parameters (ADP) yielded further lowering of the *R*-values, but not all issues pertaining to the Fourier maps were resolved by treating the atoms anisotropicaly (the magnitudes of the highest peaks and the deepest holes decreased significantly). For illustration, we provide the contour plots of the observed Fourier maps in ESI.† From the plots, it is apparent that the As4/Sb4 position might be subject to a positional disorder. Without modelling the disorder (split positions), the thermal ellipsoids are grossly elongated (see Fig. S1, ESI†). The disorder is somewhat obscure in the Sb-compounds (cigar-shaped ADP), while for the two As-compounds, the dumbbell-shaped ADP clearly pointed at a split site (the 8*b* site is slightly shifted to 16*f*, *i.e.*, two-fold split with an occupancy of 0.5/ea). Indeed, when the As4/Sb4 site was split, the refinement confirmed this notion—the distance between the pair of atoms in the split model measures ~0.4 Å for Sb and ~0.7 Å for As.

§ Tetragonal space group $I4_1/acd$ assumed in all three cases. Unit cell parameters for $Yb_{14}CdSb_{11}$: a = 16.605(3) Å, c = 22.144(7) Å; $(Yb,Ca)_{14}CdSb_{11}$: a = 16.617(3) Å, c = 22.355(9) Å; $Ba_{14}CdSb_{11}$: a = 18.527(4) Å, c = 24.102(6) Å. Further synthetic and structural work is currently in progress.

The volumes of the polyhedra and the Voronoi cells were then calculated to investigate the appropriate disordered model adopted by the structure in the Sb-compounds. From the results, discussed later on, one can conclude that the splitting does not impact the volume of the polyhedra and Voronoi cells. Therefore, $A_{14}Cd_{1+x}Sb_{11}$ (A = Eu, Sr) were refined treating Sb4 at its idealized position, while for the As-analogs, the site was split. Where applicable (non-zero occupation above 3σ), the extra Cd2 was also included in the refinements. All calculations converged smoothly to low R_1 values and with no significant electron density left in the difference Fourier map. Exception here is the $Eu_{14}CdSb_{11}$ structure, where there is a peak of 6 e^- Å^{-3} in close proximity of Eu2 (<0.8 Å), the origins of which are still not understood.

The final positional parameters were standardized using the STRUCTURE TIDY program.[27] Selected crystallographic data, atomic coordinates and isotropic equivalent displacement parameters, and important interatomic distances are presented in Tables 1–6. Additional information on the crystal structure refinements can be found from the Fachinformationszentrum Karlsruhe, 76344 Eggenstein-Leopoldshafen, Germany (fax: +49-7247-808-666; Email: crysdata@fiz-karlsruhe.de), on quoting the depository number CSD-429719 (for $Sr_{14}CdAs_{11}$); CSD-4329720 (for $Eu_{14}CdAs_{11}$); CSD-429721 (for $Sr_{14}CdSb_{11}$); and CSD-429722 (for $Eu_{14}CdSb_{11}$).

2.3 Property measurements

Temperature dependent electrical resistivity was measured from 5 to 300 K with an excitation current of 10 mA using a Quantum Design PPMS. Four platinum wires were connected to single crystals of $Eu_{14}CdAs_{11}$ using EPO TEK H20 silver epoxy. The measurements were carried out on both heating and cooling for two different crystals to ensure reproducibility.

Field-cooled direct current (dc) magnetization (M) in the temperature range of 2–300 K and an applied field of 500 Oe (H) was measured also using the PPMS. The measurements were done for two different batches to ensure reproducibility. Several flux-grown $Eu_{14}CdAs_{11}$ crystals were collected and enclosed in gel-capsules with the top filled with cotton to prevent the crystals from moving under the magnetic field. The raw magnetization data were converted to molar susceptibility ($\chi_m = M/H$). The effective magnetic moment (μ_{eff}) and Weiss temperature (θ_p) were calculated from a linear fit of the inverse magnetic susceptibility *versus* temperature.

2.4 Computational details

The electronic structure calculations for idealized $Sr_{14}CdSb_{11}$, *i.e.*, neglecting the disorder, were performed using the linear muffin-tin orbital (TB-LMTO) method[28] within the Stuttgart TB-LMTO 4.7 program.[29] The experimental unit cell parameters and atomic coordinates were employed for the calculation. The program package employs the atomic sphere approximation (ASA), in which space is filled with overlapping Wigner–Seitz

Table 1 Selected crystal data and structure refinement parameters for $Sr_{14}CdAs_{11}$ and $Eu_{14}CdAs_{11}$ (both done at 200(2) K and using monochromated MoKα radiation, λ = 0.71073 Å)

Empirical formula	$Sr_{14}Cd_{1.06(1)}As_{11}$	$Eu_{14}CdAs_{11}$
Formula weight	2169.52	3063.96
Space group, Z	$I4_1/acd$ (No. 142), 8	
a (Å)	16.615(2)	16.3057(8)
c (Å)	22.321(6)	21.860(2)
V (Å^3)	6162(2)	5812.0(7)
ρ_{cal} (g cm^{-3})	4.68	7.00
μ (cm^{-1})	364.4	428.4
Goodness-of-fit on F^2	1.06	0.95
$R_1(I > 2\sigma_I)^a$	0.028	0.027
$wR_2(I > 2\sigma_I)^a$	0.066	0.045

[a] $R_1 = \sum||F_o| - |F_c||/\sum|F_o|$; $wR_2 = [\sum[w(F_o^2 - F_c^2)^2]/\sum[w(F_o^2)^2]]^{1/2}$, where $w = 1/[\sigma^2F_o^2 + (AP)^2 + BP]$ and $P = (F_o^2 + 2F_c^2)/3$; A and B are weight coefficients. For additional information, refer to the CIF in the ESI.

Table 2 Selected crystal data and structure refinement parameters for $Sr_{14}CdSb_{11}$ and $Eu_{14}CdSb_{11}$ (both done at 200(2) K and using MoKα radiation)

Empirical formula	$Sr_{14}Cd_{1.30(1)}Sb_{11}$	$Eu_{14}Cd_{1.27(1)}Sb_{11}$
Formula weight	2712.05	3609.72
Space group, Z	$I4_1/acd$ (No. 142), 8	
a (Å)	17.616(2)	17.403(3)
c (Å)	23.203(6)	22.862(7)
V (Å^3)	7200(2)	6924(3)
ρ_{cal} (g cm^{-3})	5.00	6.93
μ (cm^{-1})	293.7	340.9
Goodness-of-fit on F^2	1.04	1.10
$R_1(I > 2\sigma_I)^a$	0.029	0.034
wR_2 $(I > 2\sigma_I)^a$	0.066	0.072

[a] $R_1 = \sum||F_o| - |F_c||/\sum|F_o|$; $wR_2 = [\sum[w(F_o^2 - F_c^2)^2]/\sum[w(F_o^2)^2]]^{1/2}$, where $w = 1/[\sigma^2F_o^2 + (AP)^2 + BP]$ and $P = (F_o^2 + 2F_c^2)/3$; A and B are weight coefficients. For additional information, refer to the CIF in the ESI.

Table 3 Atomic coordinates and equivalent isotropic displacement parameters for $Sr_{14}CdAs_{11}$ and $Eu_{14}CdAs_{11}$

Atom	Site	x	y	z	$U_{eq.}$[a] (Å^2)
$Sr_{14}CdAs_{11}$					
Sr1	32*g*	0.04283(4)	0.07250(4)	0.17177(3)	0.0237(2)
Sr2	32*g*	0.02378(4)	0.37463(4)	0.00601(3)	0.0261(2)
Sr3	16*e*	0.35067(4)	0	1/4	0.0194(2)
Sr4	32*g*	0.34883(4)	0.07405(4)	0.09541(3)	0.0284(2)
Cd1	8*a*	0	1/4	3/8	0.0197(2)
Cd2[b]	32*g*	0.4673(3)	0.0181(2)	0.0828(2)	0.023(2)
As1	16*f*	0.13431(4)	0.38431(4)	1/8	0.023(2)
As2	32*g*	0.36136(4)	0.25449(4)	0.05714(3)	0.0189(2)
As3[c]	32*g*	0.1276(8)	0.02533(5)	0.04611(4)	0.0228(4)
As4[d]	16*f*	0.01666(7)	0.26666(7)	1/8	0.0174(4)
$Eu_{14}CdAs_{11}$					
Eu1	32*g*	0.04393(2)	0.07268(2)	0.17149(2)	0.0115(9)
Eu2	32*g*	0.02365(2)	0.37581(2)	0.00433(2)	0.0129(2)
Eu3	16*e*	0.35087(3)	0	1/4	0.0120(2)
Eu4	32*g*	0.34726(3)	0.07239(2)	0.09466(2)	0.0144(1)
Cd1	8*a*	0	1/4	3/8	0.0105(2)
As1	16*f*	0.1328(5)	0.38283(5)	1/8	0.0127(2)
As2	32*g*	0.3588(5)	0.25399(5)	0.05673(3)	0.0113(2)
As3	32*g*	0.1289(5)	0.02624(5)	0.04755(3)	0.0135(2)
As4[d]	16*f*	0.0133(9)	0.26328(9)	1/8	0.0103(7)

[a] $U_{eq.}$ is defined as one-third of the trace of the orthogonalized U_{ij} tensor. [b] Occupancy of 1.6(2)%. [c] As3 experiences a small positional disorder, modelled as a majority site (above, 91%) and a minority site (As3B, x = 0.1602(9), y = 0.0370(6), z = 0.0739(8), 9%). [d] Split sites (8*b* to 16*f*) with an occupancy of 50%.

Table 4 Atomic coordinates and equivalent isotropic displacement parameters for $Sr_{14}CdSb_{11}$ and $Eu_{14}CdSb_{11}$

Atom	Site	x	y	z	$U_{eq.}$ [a] (Å^2)
$Sr_{14}CdSb_{11}$					
Sr1	32*g*	0.04254(4)	0.07391(4)	0.17206(3)	0.0188(2)
Sr2	32*g*	0.02350(4)	0.37470(4)	0.00245(3)	0.0249(2)
Sr3	16*e*	0.35384(5)	0	1/4	0.0129(2)
Sr4	32*g*	0.3434(4)	0.07215(4)	0.09414(3)	0.0236(2)
Cd1	8*a*	0	1/4	3/8	0.0157(3)
Cd2[b]	32*g*	0.4737(3)	0.0059(3)	0.0776(3)	0.0131(2)
Sb1	16*f*	0.13437(2)	0.38437(2)	1/8	0.0139(2)
Sb2	32*g*	0.35911(2)	0.25529(2)	0.06068(2)	0.0152(2)
Sb3	32*g*	0.12931(3)	0.02694(3)	0.04578(2)	0.0198(2)
Sb4	8*b*	0	1/4	1/8	0.0335(3)
$Eu_{14}CdSb_{11}$					
Eu1	32*g*	0.04302(3)	0.07384(3)	0.17185(2)	0.0174(2)
Eu2	32*g*	0.02292(3)	0.37498(4)	0.00142(3)	0.0237(2)
Eu3	16*e*	0.35437(4)	0	1/4	0.0127(2)
Eu4	32*g*	0.34214(4)	0.07138(3)	0.09403(2)	0.0229(2)
Cd1	8*a*	0	1/4	3/8	0.0152(3)
Cd2[c]	32*g*	0.4740(6)	0.0063(6)	0.078(4)	0.009(3)
Sb1	16*f*	0.13401(4)	0.38401(4)	1/8	0.0133(2)
Sb2	32*g*	0.35773(4)	0.25492(4)	0.06036(3)	0.0148(2)
Sb3	32*g*	0.12978(5)	0.02680(4)	0.04565(3)	0.0183(2)
Sb4	8*b*	0	1/4	1/8	0.027(4)

[a] $U_{eq.}$ is defined as one-third of the trace of the orthogonalized U_{ij} tensor. [b] Occupancy of 7.5(2)%. [c] Occupancy of 6.8(3)%, refined isotropically.

Table 5 Selected interatomic distances (Å) for $Sr_{14}CdAs_{11}$ and $Eu_{14}CdAs_{11}$

$Sr_{14}CdAs_{11}$		$Eu_{14}CdAs_{11}$	
Atom pair	Distance	Atom pair	Distance
Sr1–As3A/B[a]	3.213(2)/2.837(1)	Eu1–As3	3.111(1)
Sr1–As3A/B[a]	3.226(2)/2.982(1)	Eu1–As3	3.136(1)
Sr1–As1	3.204(1)	Eu1–As1	3.141(1)
Sr1–As2	3.189(1) × 2	Eu1–As2	3.114(1) × 2
Sr1–As4	3.418(2)	Eu1–As4	3.308(2)
Sr1–Sr1	3.791(2)	Eu1–Eu1	3.689(1)
Sr1–Sr3	3.833(2)	Eu1–Eu3	3.776(1)
Sr1–Sr4	3.625(1)	Eu1–Eu4	3.543(1)
Sr2–As1	3.233(1)	Eu2–As1	3.184(1)
Sr2–As2	3.101(1)	Eu2–As2	3.066(1)
Sr2–As3A[a]	3.147(2)	Eu2–As3	3.103(1)
Sr2–As3A[a]	3.257(1)	Eu2–As3	3.201(1)
Sr2–As4	3.208(2)	Eu2–As4	3.217(1)
Sr2–Sr1	3.953(1)	Eu2–Eu1	3.908(1) × 2
Sr2–Sr3	3.783(1)	Eu2–Eu3	3.711(1)
Sr2–Sr4	3.782(2)	Eu2–Eu4	3.697(1)
Sr3–As3A/B[a]	3.093(1)/3.197(1) × 2	Eu3–As3	3.046(1) × 2
Sr3–As1	3.397(1) × 2	Eu3–As1	3.345(1) × 2
Sr3–As2	3.293(1) × 2	Eu3–As2	3.207(1) × 2
Sr3–Sr4	3.664(1) × 2	Eu3–Eu4	3.595(1) × 2
Sr4–As3A[a]	3.283(1) × 2	Eu4–As3	3.222(1) × 2
Sr4–As1	3.233(2)	Eu4–As1	3.178(1)
Sr4–As2	3.124(1)	Eu4–As2	3.081(1)
Sr4–As2	3.325(1)	Eu4–As2	3.299(1)
Cd1–As2	2.758(1) × 4	Cd1–As2	2.745(1) × 4
Cd1–Sr2	3.605(1) × 4	Cd1–Eu2	3.514(1) × 4
As1–As4	2.764(1)	As1–As4	2.757(2)
As3B–As3B[a]	2.552(3)		

[a] As3 experiences a small positional disorder, modelled as a majority site (As3A, 91%) and a minority site (As3B, 9%).

Table 6 Selected interatomic distances (Å) for $Sr_{14}CdSb_{11}$ and $Eu_{14}CdSb_{11}$

$Sr_{14}CdSb_{11}$		$Eu_{14}CdSb_{11}$	
Atom pair	Distance	Atom pair	Distance
Sr1–Sb3	3.369(1)	Eu1–Sb3	3.322(2)
Sr1–Sb3	3.407(1)	Eu1–Sb3	3.358(2)
Sr1–Sb1	3.383(1)	Eu1–Sb1	3.343(1)
Sr1–Sb2	3.382(2) × 2	Eu1–Sb2	3.327(2) × 2
Sr1–Sb4	3.373(1)	Eu1–Sb4	3.333(1)
Sr1–Sr1	3.980(2)	Eu1–Eu1	3.915(2)
Sr1–Sr3	4.002(1)	Eu1–Eu3	3.952(1)
Sr1–Sr4	3.809(2)	Eu1–Eu4	3.747(2)
Sr2–Sb1	3.454(1)	Eu2–Sb1	3.427(1)
Sr2–Sb2	3.293(1)	Eu2–Sb2	3.267(1)
Sr2–Sb3	3.355(1)	Eu2–Sb3	3.317(2)
Sr2–Sb3	3.452(1)	Eu2–Sb3	3.405(2)
Sr2–Sb4	3.617(1)	Eu2–Sb4	3.588(1)
Sr2–Sr1	4.186(2)	Eu2–Eu1	4.137(1)
Sr2–Sr3	4.008(1)	Eu2–Eu3	3.968(1)
Sr2–Sr4	3.995(2)	Eu2–Eu4	3.941(2)
Sr3–Sb3	3.310(1) × 2	Eu3–Sb3	3.268(1) × 2
Sr3–Sb1	3.550(1) × 2	Eu3–Sb1	3.505(1) × 2
Sr3–Sb2	3.440(1) × 2	Eu3–Sb2	3.379(1) × 2
Sr3–Sr4	3.838(2) × 2	Eu3–Eu4	3.782(2) × 2
Sr4–Sb3	3.428(1) × 2	Eu4–Sb3	3.372(2) × 2
Sr4–Sb1	3.407(1)	Eu4–Sb1	3.363(2)
Sr4–Sb2	3.329(1)	Eu4–Sb2	3.297(1)
Sr4–Sb2	3.522(1)	Eu4–Sb2	3.502(1)
Cd1–Sb2	2.898(1) × 4	Cd1–Sb2	2.885(1) × 4
Cd1–Sr2	3.707(1) × 4	Cd1–Eu2	3.639(1) × 4
Cd2[a]–Sb1	3.068(6)	Cd2[b]–Sb1	3.035(10)
Cd2[a]–Sb2	3.187(6)	Cd2[b]–Sb2	3.124(10)
Cd2[a]–Sb3	2.898(6)	Cd2[b]–Sb3	2.869(10)
Cd2[a]–Sb3	3.410(1)	Cd2[b]–Sb3	3.375(10)
Cd2[a]–Sr1	2.872(6)	Cd2[b]–Eu1	2.826(10)
Cd2[a]–Sr2	2.896(7)	Cd2[b]–Eu2	2.879(10)
Cd2[a]–Sr2	2.940(6)	Cd2[b]–Eu2	2.881(10)
Cd2[a]–Sr4	2.603(6)	Cd2[b]–Eu4	2.585(10)

[a] Occupancy of 7.5(2)%. [b] Occupancy of 6.8(3)%.

(WS) atomic spheres.[30] Exchange and correlation were treated by the local density approximation (LDA).[31] All relativistic effects except spin–orbit coupling were taken into account by using a scalar relativistic approximation.[32] In the ASA method, the symmetry of the potential is considered spherical inside each WS sphere, and a combined correction is used to take into account the overlapping part. The radii of WS spheres were obtained by requiring that the overlapping potential be the best possible approximation to the full potential, and were determined by an automatic procedure. This overlap should not be too large because the error in kinetic energy introduced by the combined correction is proportional to the fourth power of the relative sphere overlap. No empty spheres were used. The following WS radii—Sr = 2.06–2.08 Å, Cd = 1.65 Å, Sb = 1.81–1.98 Å—were used for the calculation. The basis sets included 5d, 6s, and (6p) orbitals for Sr; 4d, 5s, and 5p orbitals for Cd; 5s, 5p, and (5d) orbitals for Sb. The downfolded orbitals (in parentheses) were treated by the Löwdin downfolding technique.[33] The Cd 4d orbitals were treated as core wave functions. For bonding analysis, the energy contributions of all filled electronic states for selected atom pairs were calculated by the crystal orbital Hamilton population (COHP) method.[34] The *k*-space integrations were conducted by the tetrahedron method,[35] and the self-consistent charge density was obtained using consistent irreducible *k*-points in the Brillouin zone.

3 Results and discussion

3.1 Crystal chemistry

During our continuous effort to provide insight into the interplay between the size and electronic effects in the "$A_9M_{4+x}Pn_9$" family[18] (A = Ca, Sr, Eu, or Yb; Pn = Sb, Bi; and M = Mn, Zn, Cd), we serendipitously (re)discovered $Sr_{14}Cd_{1.30(1)}Sb_{11}$. This structure is the very same one which the Kauzlarich group identified as $Sr_{14}CdSb_{11.37}$,[12] with the difference being the interpretation of the additional interstitial atoms. We assigned the interstitial atoms as Cd, much like M is filled in $A_9M_{4+x}Pn_9$, whereas the original report on the Sr–Cd–Sb phase assumed the atom at the interstitial site to be antimony.[12] Since this structure is familiar, the following discussion will focus primarily on an alternative description and the arguments in favor of the notion that from both geometric and electronic standpoints, Cd^{2+} will be preferred over Sb^{3-} as an interstitial species.

The stoichiometric and non-stoichiometric compounds in the series $A_{14}Cd_{1+x}Pn_{11}$ (A = Sr, Eu; Pn = As, Sb) adopt the $Ca_{14}AlSb_{11}$ structure type[2] which crystallizes in the tetragonal unit cell with space group $I4_1/acd$ (Pearson code $tI208$).[36] The structure of these compounds is not simple, but can be readily visualized as made of $[CdPn_4]$ tetrahedra, linear Pn_3-units and isolated Pn atoms as shown in Fig. 1 and 2. Based on the split of the As4 site in particular, as described above, and as shown in Fig. S1 (ESI†), one can argue that the structure of $A_{14}CdAs_{11}$ (A = Sr, Eu) does not have trimeric As_3, and instead features an As_2-dimer and an isolated As ion. This split atomic position is less apparent in $A_{14}Cd_{1+x}Sb_{11}$ (A = Sr, Eu)—recall that the distance between the split sites is less than 0.4 Å for the antimonides and over 0.7 Å for the As-analogs.

The average As–As distance in the dumbbell measures 2.761(1) Å and compares well with similar distances in $Ca_{14}GaAs_{11}$[8] and $Eu_{14}MnAs_{11}$.[37] However, these homoatomic interactions appear to be longer than the sum of the covalent radii between As atoms (2.42 Å),[38] or other previously reported compounds, $Ba_2Cd_2As_3$ (2.49 Å)[39] and $Ba_4Li_2Cd_3As_6$ (2.51 Å).[40] The As4 and As1, which are atoms of the dumbbell, are located near the center of a tri-capped trigonal prism coordinated with eight Sr or Eu atoms and one As atom (Fig. 1D). The As–A (A = Sr, Eu) distances within these polyhedra are distributed between 3.204(1) and 3.397(1) Å (average 3.30(1) Å) for Sr, and between 3.141(1) and 3.345(1) Å (average 3.243(1) Å) for Eu. These distances are of the same order with similar contacts as in other previously reported compounds.[12,17,37]

Having discussed the bonding interactions within the As1 and As4 polyhedra, we turn now our attention to the Sb1 and Sb4 local environments. Recall that these two atoms form the $[Sb_3]^{7-}$ unit. Sb1 and Sb4 atoms are located at the centers of polyhedra of ten and eleven Sr and Cd neighbors, as shown in Fig. 3. The Sb1–Sb4 bond in the trimer is very long (3.34 Å), which is not typical for the Sb–Sb single bond (expected value *ca.* 2.8 Å).[38] The Sb1–A (A = Sr, Eu) contacts range from 3.383(1) to 3.550(1) Å and from 3.343(1) to 3.505(1) Å for the Sr- and the Eu-analog, respectively. The Sb1–Cd2 bonds measure 3.068(6) Å and 3.035(10) Å in $Sr_{14}CdSb_{11}$ and $Eu_{14}CdSb_{11}$, respectively. These bonds match the expected heteroatomic single-bond value (2.9 Å).[38] The Sb4–Sr and Sb4–Eu distances fall in the range 3.373(1)–3.617(1) Å and 3.333(1)–3.588(1) Å, respectively.

The coordination polyhedra of the two types of Cd atoms are worthy of a special mention too. One should note here that we included exclusively atoms of the first coordination sphere involving only covalent bonds. Under this approximation, the Cd atoms form a polyhedron consisting of an inner $[CdPn_4]$ and an outer $[CdA_4]$ tetrahedron (Fig. 1D and 3C). This polyhedron bears resemblance to the tetrahedral unit substructure of the gamma-brass cluster (Fig. 4A), which is a structural building

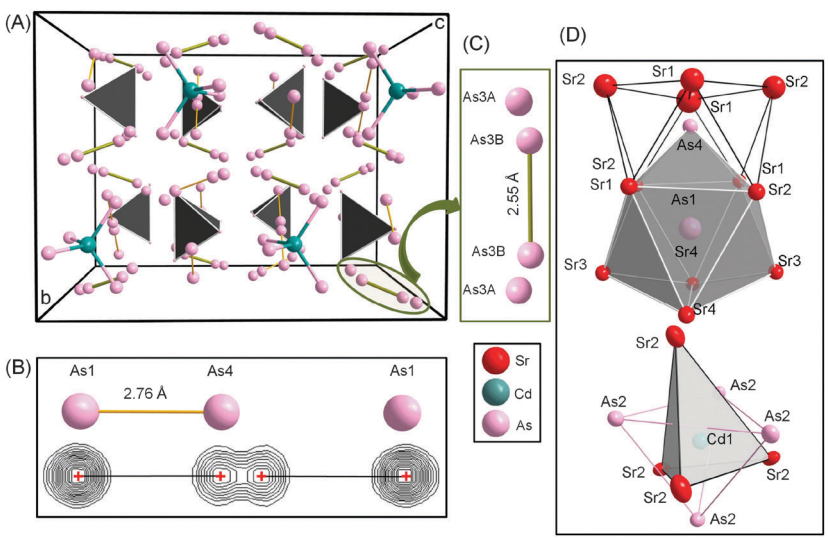

Fig. 1 (A) A representation of the structure of $Sr_{14}CdAs_{11}$ (Sr atoms omitted for clarity) showing $[CdAs_4]$ tetrahedra, isolated As atoms and the linear hypervalent $[As_3]^{7-}$ anion. (B) Cutouts of a ball and stick representation (top) and observed Fourier electron density (bottom) from the refined atomic positions of the hypervalent anion in the structure of $Sr_{14}CdAs_{11}$ (see Fig. S1 in ESI†). (C) Positional disorder involving the isolated As3 atom. Taking the disorder into consideration, a possible formation of As_2-dumbbell can be envisioned. (D) Coordination polyhedra of As1 and As4 atoms of the hypervalent anion (top); coordination polyhedron of Cd1 atoms (bottom).

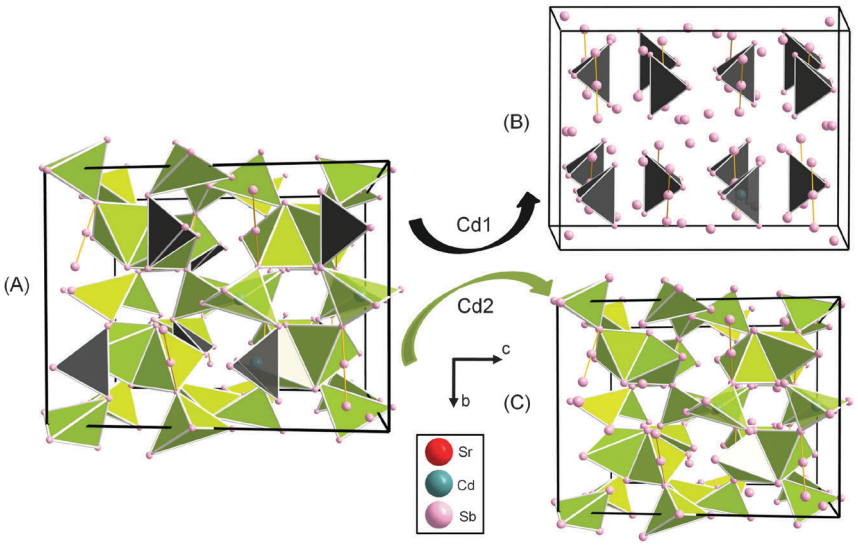

Fig. 2 (A) A projection of the crystal structure of $Sr_{14}CdSb_{11}$ viewed approx. along the *a*-axis showing a framework of $[CdSb_4]$ tetrahedra, isolated Sb atoms and the linear hypervalent $[Sb_3]^{7-}$ anion. (B) Isolated Cd1 tetrahedra. (C) Framework of edge- and corner-sharing $[Cd(2)Sb_4]$ tetrahedra. The Sr atoms are omitted for clarity.

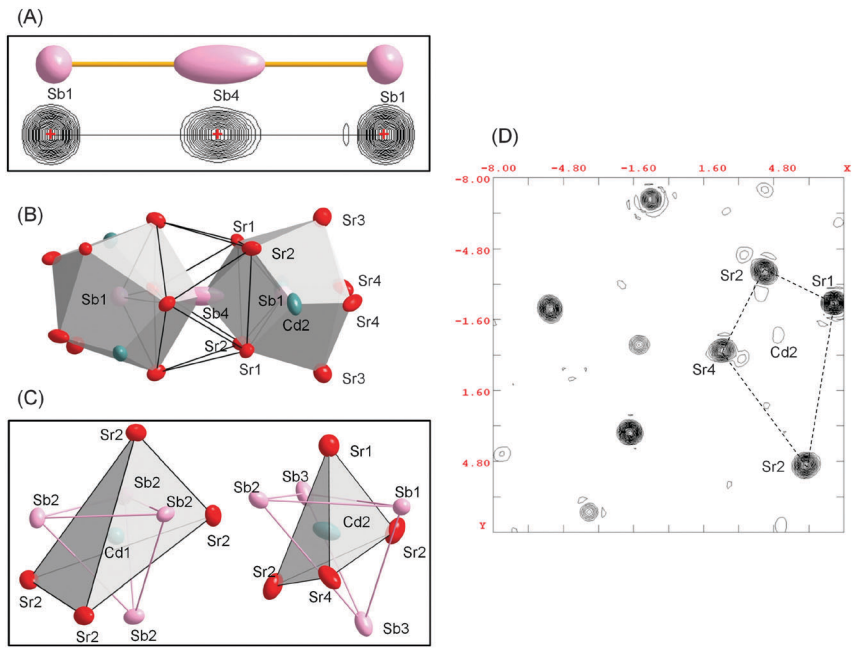

Fig. 3 (A) Cutouts of a ball and stick representation (top) and observed Fourier electron density (bottom) from the refined atomic positions of the hypervalent anion in the structure of $Sr_{14}CdSb_{11}$ (see details in Fig. S1 in ESI†). (B) Coordination polyhedra of Sb1 and Sb4 atoms of the hypervalent anion. (C) Coordination polyhedron of Cd1 and Cd2 atoms (bottom). (D) Contour plot scaled in 8 × 8 Å of the observed Fourier electron density (3–6 e^- $Å^{-3}$) from the refined positions of Sr atoms around Cd2.

block in many intermetallic compounds.[41–45] This tetrahedral unit is also known as "tetraederstern".[41] Let us recall that in the gamma-brass cluster, four interpenetrating icosahedra (each centered on the atom of the inner tetrahedron) share a common tetrahedron. Yet, the icosahedra of the outer tetrahedron offer a different geometrical configuration—they share face with each other and with a central tetrahedron. Such atomic arrangement is known as augmented gamma-brass or Pearce cluster.[41,46–50] It is important to note that the bond distance between the Zn atoms (2.7 Å) in this subunit of the gamma-brass cluster compares well with the homoatomic single-bond (2.66 Å).[38] Importantly, those clusters are well known to have the ability to host many interstitial atoms, particularly light elements such as C, H, O.

Let us now discuss the bonding interactions within the Cd polyhedron. First, we should note that there is no close contact

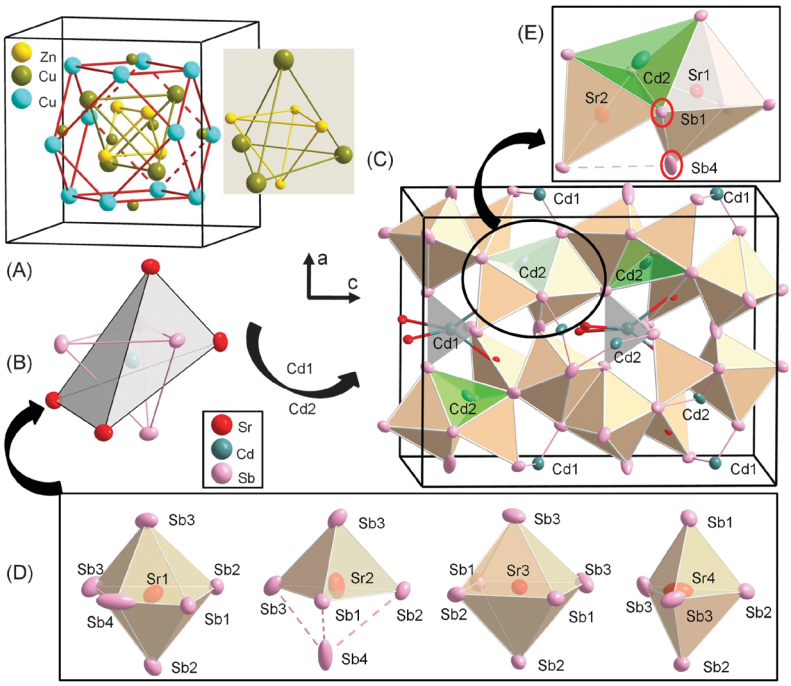

Fig. 4 Alternative description of the crystal structure of $Sr_{14}CdSb_{11}$ using a small set of coordination polyhedra of the electropositive metal atoms and taking advantage of the resemblance of the Cd polyhedra (A, right) to the "tetraederstern" substructure of the gamma-brass cluster (A, left). (B) First coordination sphere of Cd atoms forming a filled distorted "tetraederstern" consisting of an inner $[CdSb_4]$ and an outer $[CdSr_4]$ tetrahedron. (C) A projection of the structure of $Sr_{14}CdSb_{11}$ regarded as a space-filling packing of first coordination spheres of Sr atoms forming distorted octahedra and trigonal bipyramids shown in (D). (E) A complex packing showing how the inner $[CdSb_4]$ tetrahedron shares faces with distorted octahedra and trigonal bipyramids of Sr atoms. Two such polyhedra are omitted for the sake of clarity. Not only does this packing help to study the interplay between the size of the "free volume" to accommodate the excess Cd atoms (Cd2) and the instability of the linear hypervalent, but also to explain the relatively short cation–cation contacts in the structure with respect to the Pauling's third rule.

between the As or Sb atoms within the sphere of the inner tetrahedron. Their homoatomic distances measure 4.44 and 4.61 Å, respectively, which is almost the double of their corresponding single-bond distance.[38] The average Cd1–As2 and Cd1–Sr2/Eu2 distances are 2.750(1) Å and 3.605(1) Å for $Sr_{14}CdAs_{11}$, and 2.745(1) Å and 3.595(1) Å for $Eu_{14}CdAs_{11}$, respectively. Similarly, the average Cd2–Sb distances are 3.239(5) Å in $Sr_{14}CdSb_{11}$ and 3.205(10) Å in $Eu_{14}CdSb_{11}$, respectively. The average Cd2–Sr and Cd2–Eu distances, however, are unreasonably short, *ca.* 2.7 Å, which must be an artefact of the very low occupancy of the Cd2 position.¶ Apparently, the distances involving Cd2 cannot be established reliably by single-crystal X-ray diffraction, as demonstrated previously on the examples of $A_9M_{4+x}Pn_9$, where A denotes Ca, Sr, Eu, or Yb and Pn = Sb, Bi,[18] which are structurally related in terms of containing additional M-atoms (M = Mn, Zn or Cd) at the interstitial sites. It was therefore imperative to look for an alternative description of this structure in order to shed some light on the origin of those bonding interactions.

If we consider the $[CdPn_4]$ and $[CdA_4]$ tetrahedra (Fig. 4B) and the first coordination sphere polyhedra of the A^{2+} cations shown in Fig. 4D—a distorted $[APn_6]$ octahedron, $[APn_5]$ trigonal bipyramid—the structure can be described in a different way. This structural description model is not only based on a simple geometrical arrangement of atoms, which, of course, is essential to understanding (or visualizing) crystal structures and structural relationships, but also takes into account the covalent bonding interaction. The structure can then be regarded as space-filling packing of distorted $[APn_6]$ octahedra and $[APn_5]$ trigonal bipyramids. The Cd atoms are located in the interstitial sites forming a complex unit of inner $[CdPn_4]$ and outer $[CdA_4]$ tetrahedra, as depicted in Fig. 4C.

The $[Cd(1)Pn_4]$ tetrahedra (Fig. 1D and 3C) share edges and corners with the $[APn_5]$ (A = Eu, Sr) trigonal bipyramid (Fig. 4D and Fig. S3, ESI†), whereas the $[Cd(2)Pn_4]$ tetrahedra share edges with distorted $[APn_6]$ octahedra and $[APn_5]$ trigonal bipyramids (Fig. 4D and Fig. S3, ESI†). This structural topology of face and edge sharing polyhedra highlighted in Fig. 4E helps to understand the origin of the robust cation–cation bonds. After all, these findings seem to be in accordance with the Pauling's third rule.[38b] As we noted earlier, such interactions are not without precedent and were already observed in other previously reported compounds such as $A_9Zn_{4+x}Pn_9$ and $A_9Cd_{4+x}Pn_9$,[18,51] where A denotes Ca, Sr, Eu, or Yb and Pn = Sb, Bi, $Yb_9Mn_{4+x}Pn_9$,[52] and $Ca_9Mn_{4+x}Sb_9$,[53] among others. Of course,

¶ In $Sr_{14}CdSb_{11.37}$ (ref. 12), which we argue is the same material as $Sr_{14}Cd_{1.30(1)}Sb_{11}$ reported herein, the disorder is the same, but the interpretation is different. The distances of the reported interstitial Sb to its closest neighbors are of the same order as the distances we refine between Cd2 and its closest neighbors. Apparently, assigning Cd^{2+} or Sb^{3-} to the interstitial site cannot be made based on crystallographic data. In this work, we argue that Cd^{2+} is the likely interstitial species, *i.e.*, the formula of the compound is $Sr_{14}Cd_{1+x}Sb_{11}$.

these structures can also be regarded as space-filling arrangement of distorted [APn_6] octahedra and [APn_5] square pyramids. An illustration is shown in ESI† (Fig. S4 and S5). The Cd atoms occupy the interstitial sites forming distorted [$CdBi_4$] tetrahedra sharing edges and faces with the neighboring distorted [$CaBi_6$] octahedra and [$CaBi_5$] square pyramids. Finally, it is important to note that the structure of the $A_9M_{4+x}Pn_9$ family offers more structural flexibility to accommodate new cationic species leading to stuffed variant compounds as evidenced by the recent report of Kazem *et al.*[54] In the next sections we will attempt to gain further insights into two main questions: (1) why the interstitial chemistry in $A_{14}M_{1+x}Pn_{11}$ appears to be limited to the Sb-compounds, while the As-analogs show very little or no occupation at the interstitial site (but show different types of structural distortions/variances)? and (2) given the very low electron density at the interstitial position and the lack of conclusive evidence from the interatomic distances,¶ would the formula $A_{14}M_{1+x}Pn_{11}$ (*i.e.*, interstitial site filled by Cd^{2+}) or $A_{14}MPn_{11+x}$[12] (*i.e.*, assign Sb^{3-} to the interstitial site) be more reasonable?

From simple structural considerations, as illustrated above, it seems reasonable that the geometric factors might have more implication in the formation of these nonstoichiometric compounds. In order to provide rigorous support to this argument, it will be instructing to evaluate how the volume of the unit cell should be divided up between the different constituents, Cd, Pn and A atoms (Pn = As, Sb; A = Eu, Sr), of the structure. A hard sphere approach can be immediately rejected since it accounts for less than 50% of the unit cell volume. A more reasonable method used to evaluate the effective atomic volume is based on the Voronoi cell approach.‖ This method[55] has been successfully used as a standard method for (1) the calculation of volumes of protein constituents, the description of protein motions, and the analysis of cavities in proteins,[56] (2) for climate system and global modeling,[57] (3) the analysis of computational molecular simulations,[58] and (4) for allocation of space among atoms.[59] In this study, the volume of Voronoi domains (or cell) and that of coordination polyhedra were accessed employing the NRCVAX software package.[60]

The calculated volumes of coordination polyhedra and the Voronoi cell are presented in Table 7 for some selected atoms. The results are quite consistent with the expected trends, and more specifically, for the Cd2 atoms, the volume of the eight-coordinated polyhedron can be seen to decrease slightly from 73.75 to 70.87 Å^3 and that of the Voronoi cell from 22.22 to 21.39 Å^3 with the decrease in the size of the cations in $Sr_{14}CdSb_{11}$ (Sr^{2+} with r = 1.18 Å)[61] and $Eu_{14}CdSb_{11}$ (Eu^{2+} with r = 1.17 Å),[61] respectively. In contrast, when considering $Sr_{14}CdSb_{11}$ and $Sr_{14}CdAs_{11}$, the volume of the coordination polyhedron drastically decreases from 73.75 Å^3 to 56.43 Å^3, and the Voronoi cell volume decreases from 22.22 Å^3 to 19.40 Å^3 with the decrease in the size of the pnictogen atom. It should be noted that the Cd2 position was found empty (*i.e.*, 0% occupancy) in $Eu_{14}CdAs_{11}$ meaning that there is insufficient volume to accommodate even a small fraction of Cd2 atoms, as seen for the other three compounds. This supports the argument that the filling of the interstitial site in this structure is very sensitive to the size of the pnictogen atoms and to some extent the counter-cation (Eu, Sr). We should also mention here that these arguments call for additional structural work, and perhaps, for the revision of some older results—notice that Zn and Mg have similar ionic size, Zn^{2+} (r = 0.60 Å); Mg^{2+} (r = 0.57 Å),[61] yet variable stoichiometry is only reported for the $Ca_{14}MSb_{11}$ compound with M = Zn, while the $Ca_{14}MSb_{11}$ compound with M = Mg displays no additional interstitial atom. One will also notice that $Yb_{14}ZnSb_{11}$ is reported to be stoichiometric (albeit Yb^{2+}/Yb^{3+} mixed-valent),[1f] while its Ca-counterpart, despite the virtually identical radii for Ca^{2+} (r = 1.01 Å)[61] and Yb^{2+} (r = 1.00 Å),[61] is sub-stoichiometric. On the other hand, the pair $Yb_{14}MgSb_{11}$ and $Yb_{14}ZnSb_{11}$ is reportedly isotypic, but not isoelectronic, as only the latter is mixed-valent.

One can also notice that the [$CdPn_4$] tetrahedra appear more distorted for the Sb-compounds than in their As-analogs. For example, the largest Pn–Cd–Pn angle in $Sr_{14}Cd_{1.06(1)}As_{11}$ is 113.4°, while the corresponding Sb–Cd–Sb angle is 118.0° (in the antimonide with the same cation, *i.e.*, in $Sr_{14}Cd_{1.30(1)}Sb_{11}$).

Table 7 Volumes of coordination type polyhedra (CP) and Voronoi cells (VC) of selected atoms in the crystal structure of $A_{14}Cd_{1+x}Pn_{11}$ (A = Sr, Eu; Pn = As, Sb); the coordination number (CN) for each atom is also given; all the volumes are given in Å^3

Atom	Volume	$Sr_{14}CdAs_{11}$	$Eu_{14}CdAs_{11}$	$Sr_{14}CdSb_{11}$	$Eu_{14}CdSb_{11}$
Cd1	CP	99.48	95.32	116.30	112.70
CN8	VC	25.07	24.12	28.50	27.67
Cd2	CP	56.43		73.75	70.87
CN8	VC	19.40		22.22	21.39
As1	CP	67.32	64.20		
CN9	VC	26.43	25.15		
As4	CP	77.50	73.96		
CN9	VC	26.23	25.05		
Sb1	CP			86.95	84.10
CN11	VC			28.56	27.55
Sb4	CP			92.22	89.33
				92.22[a]	89.33[a]
CN10	VC			31.44	30.42
				31.36[a]	30.37[a]

[a] Taking into account the possible split position.

‖ The Voronoi cell method consists of partitioning the entire space among a collection of equal-sized atoms. Each atom is surrounded by a polyhedron with its volume assigned to the atom. The faces of Voronoi polyhedra are derived from the separating planes perpendicular to the interatomic vectors, whereas the edges of the polyhedra are formed by the intersection of these planes. The Voronoi procedure requires the location of all atomic neighbors and a definition of the division points on the interatomic vectors. In this article, the volume of Voronoi Cell was calculated using the NRCVAX software package. The unit cell parameters and the atomic coordinates for all the compounds were used for precise volume calculations. As indicated in the manuscript, we seek to fill the space so that the sum of Voronoi cell volumes matches with the unit cell volume. To achieve accurate volume calculations, emphasis has been placed on the influence of the radii to assess avoidable errors since there are atoms showing different radii and regions with varying local atomic density. The total volume was computed with atomic radii in the range of 1.2–1.8 Å.

These differences can be linked to small structural distortions in response to the occupation of the available "free volume" with a small fraction of Cd atoms. This seems to be a natural response of the structure to optimize both the crystal packing and the Cd–Sb covalent bonding. A remarkably similar effect was recently reported for the series $RELi_xSn_2$ (RE = La–Nd)[62] in which it was found that the decrease of Li content in the $RESn_2$ sub-structure (*i.e.*, trigonal prism cavities) was due to the limited available "free volume" within these cavities as a result of the lanthanide contraction. In contrast, the structural analysis of the series $Ba_4Cd_3Li_2Pn_6$ (Pn = P, As, Sb)[40] recently reported by us revealed structural vacancies at the Cd and Li sub-lattice promoting thereby an interplay between ionicity and covalency among the electronegative components.

In summary, we have shown that the size of the pnictogen and highly electropositive metal atoms is an important factor for the formation of non-stoichiometric compositions. One should remember that, in principle, the occupation of a given empty position will be determined by the match between the volume of the guest atom and the site volume. This holds true also when contact areas are greater between adjacent atoms of elements that bind strongly with each other. On the basis of volume calculations, one can argue for instance that the Voronoi cell volume of Cd^{2+} (0.78 Å)[61] in $Sr_{14}CdAs_{11}$ and $A_{14}CdSb_{11}$ (A = Eu, Sr) is clearly at its maximum. Therefore, filling the interstitial site with Sb^{3-} (much larger than Cd^{2+}), as it was assigned in an early report for $A_{14}CdSb_{11+x}$ (A = Ca, Sr),[12] seems not appropriate because these atoms will not fill all the available space. This suggests that Cd^{2+} should be preferred to Sb^{3-} as a "filler" because of the space requirement and the minimization of the electrostatic effects, which is consistent with cumulative size and electronic effects recently reported for in $Sr_9Cd_{4.49}Sb_9$.[18] On the other hand, an accumulation of Sb^{3-} may render the $[SbSb_4]$ tetrahedron unstable because of the electrostatic effects, which need to be minimized in order for the crystal to achieve minimum energy. All of the above raise concerns about the nature of chemical bonding involving the interstitial atoms.

3.2 On the electronic structure and the origin of interstitial solid solutions

According to the Zintl concept,[3] and following the valence electron count in $Ca_{14}AlSb_{11}$,[2] the overall formula unit of idealized $Sr_{14}CdSb_{11}$ (neglecting the partially occupied interstitial) can be partitioned in four different entities as follows: $14x[Sr^{2+}] + [CdSb_4]^{10-} + [Sb_3]^{7-} + 4x[Sb]^{3-}$. Such electron counting reveals a charge-imbalance, since there is one missing positive charge to counterbalance the 29 electrons needed for covalent bonding within the anionic substructure. The electronic structure calculations (Fig. 5) for stoichiometric $Sr_{14}CdSb_{11}$ indicate that such structure will not be electronically stable since the Fermi level is at a substantial density of states (DOS) level, while it appears that the top of the valence band could be shifted up (by virtue of filling an extra electron) to the edge of an energy gap. A similar electronic structure was also reported for the isostructural and isoelectronic $Ca_{14}MgSb_{11}$.[11] Consequently, $Sr_{14}CdSb_{11}$ will not have fully optimized bonding and will be expected to be (semi)metallic (or degenerate semiconductor due to intrinsic disorder). The Fermi level for the disorder-free $Sr_{14}CdSb_{11}$ falls within the top of the valence band in a region of relatively high DOS (Fig. 5). The corresponding number of valence electrons is 85 per formula unit (14×2 provided by the Sr atoms, 1×2 provided by the Cd atom, and 11×5 provided by the Sb atoms). The full and partial DOS diagrams suggest that increasing the number of electrons to 86 per formula will lead to an optimal number of valence electrons. This valence electron count can come about by the addition of exactly one-half Cd atom, *i.e.*, $Sr_{14}Cd_{1.5}Sb_{11}$. This also means that $Sr_{14}Cd_{1+x}Sb_{11}$ ($x \approx 0.3$) will be slightly electron-deficient, but very close to being a valence-precise compound.

The partial DOS for Cd and Sb (Fig. 5) shows that adding excess Cd will reduce more Sb, which in turn will push the Fermi level up towards the edge of the valence band. Notice as well that according to the partial DOS of the Sr atoms, this shift might also require a slight doping (*i.e.*, dumping electrons) at the Sr sub-lattice. In either case, covalent bonding, both Cd–Sb and Sr–Sb, is optimized, as evident from the COHP diagram depicted in Fig. 6.

According to the DOS diagrams (Fig. 5), increasing the number of electrons to 86 per formula pushes the Fermi level toward the edge of the valence band. This means that if one were to obtain $A_{14}Cd_{1.5}Sb_{11}$, an intrinsic semiconductor material should be realized; any other composition will be close, but will not correspond to a true valence compound. Clear support of the notion that $A_{14}Cd_{1+x}Pn_{11}$ ($x \ll 0.5$) is not a semiconductor is

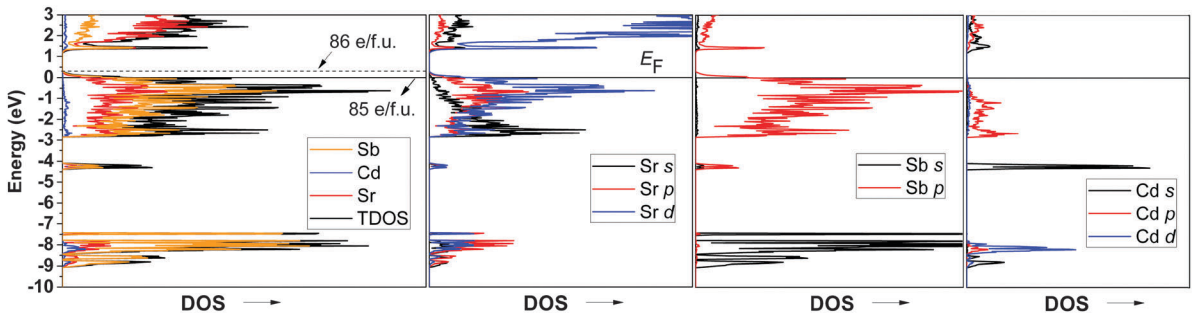

Fig. 5 Calculated total density of states (DOS) and partial density of states (PDOS) curves for the idealized compound $Sr_{14}CdSb_{11}$. The Fermi level is the energy reference at 0 eV. The three PDOS plots show the s, p, and d bands contribution for Sr, Sb (s and p bands), and Cd.

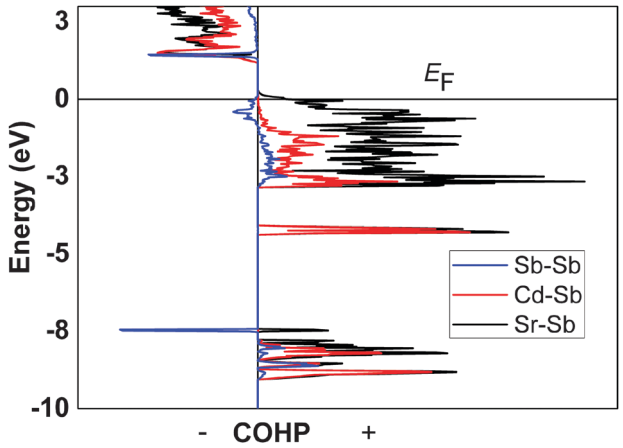

Fig. 6 Calculated total COHP curves for the average Sb–Sb, Cd–Sb, and Sr–Sb interactions in $Sr_{14}CdSb_{11}$. Since −COHP is plotted, the positive and negative signs represent bonding and antibonding states, respectively.

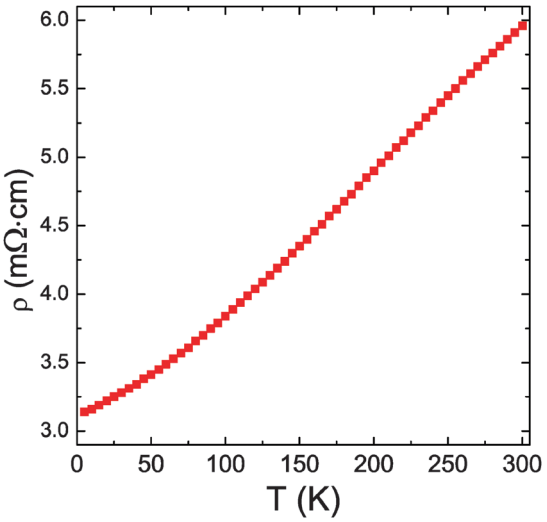

Fig. 7 Resistivity *versus* temperature of $Eu_{14}CdAs_{11}$.

obtained from the metallic electrical resistivity of $Eu_{14}Cd_{1.06(1)}As_{11}$ (Fig. 7—note that the measurement was performed on a very small single-crystal). Let us recall that the single-crystals of $Eu_{14}Cd_{1.06(1)}As_{11}$ were grown from a flux reaction, and although the ideal composition $Eu_{14}Cd_{1.5}As_{11}$ was intended, it could not be attained. This means that using the Zintl–Klemm concept, one could attempt other dopants to sway the structure–property relationships in $A_{14}Cd_{1+x}Pn_{11}$ in a targeted fashion towards obtaining more or less conductive material.

3.3 Magnetic susceptibility

The temperature dependent molar magnetic susceptibility χ and the inverse susceptibility $1/\chi$ of $Eu_{14}CdAs_{11}$ are shown in Fig. 8. $Eu_{14}CdSb_{11}$ was not phase-pure and could not be measured. The magnetic susceptibility gradually increases upon cooling to approximately 30 K. As the temperature decreases further, the susceptibility exponentially increases up to around 8 K, at which point a sharp downturn is observed.

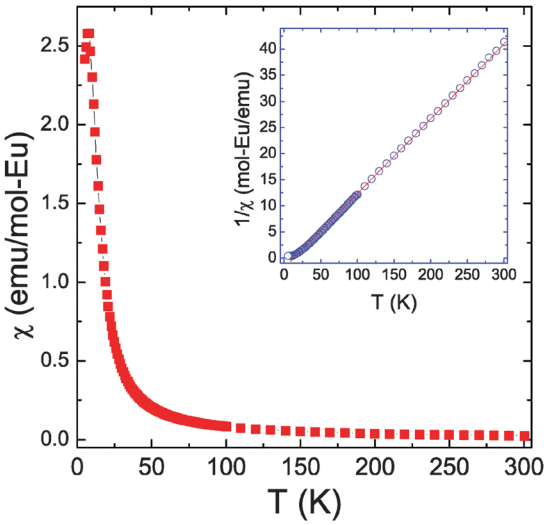

Fig. 8 Field-cooled magnetic susceptibility *versus* temperature of $Eu_{14}CdAs_{11}$ (data normalized per Eu). The plot shown in the inset is the temperature dependence of the inverse magnetic susceptibility and the linear fit to the Curie–Weiss law.

This steep increase in magnetic susceptibility can be tentatively ascribed to a ferromagnetic (FM) ordering transition with a Curie temperature T_C = 30 K (obtained from the mid-point of the first derivative plot of χ *vs.* T). The second feature in the magnetic susceptibility data could be attributed to a successive ordering transition, which is likely antiferromagnetic (AFM). There is only limited data gathered below the speculated AFM transition, but we could argue that the χ *vs.* T seems to be mirroring the susceptibility data for the isotypic $Eu_{14}MnP_{11}$ and $Eu_{14}MnAs_{11}$,[37] which also show similar magnetic transition. The high-temperature regime of the inverse susceptibility can be fitted to the Curie–Weiss law, $\chi = C/(T - \theta_p)$. The fit results in an effective magnetic moment, μ_{eff} = 28.0 μ_B/f.u. (μ_{eff} = 7.5 μ_B/Eu), and a paramagnetic Weiss temperature, θ_p = 13 K.

The calculated effective magnetic moment is very close to the expected theoretical value (7.94 μ_B) of Eu^{2+} free-ions, and is consistent with the previously reported results for $Eu_{14}MnAs_{11}$.[37] The magnetic ordering of the Eu spins confirms that the atoms participate in "clustering", which is consistent with our structural description of a "tetraederstern" cluster consisting of inner $CdAs_4$ and outer $CdEu_4$ tetrahedra as described above. The positive value of θ_p agrees with the presumed ferromagnetic ordering, and one can notice that θ_p for $Eu_{14}CdAs_{11}$ is lower than the one obtained for $Eu_{14}MnAs_{11}$ (θ_p = 71 K).[37] This may be suggestive of weakened ferromagnetic Eu–Eu interactions in $Eu_{14}CdAs_{11}$, due to the smaller unit cell parameters of $Eu_{14}MnAs_{11}$, and correspondingly, shorter Eu–Eu contacts. Of course, it is also possible that $Eu_{14}CdAs_{11}$ lacks the Mn-sublattice, which might synergistically mediate the Eu–Eu interactions.

Such complex packing can result in a cooperative ferromagnetic order due to geometrical spin frustration in the magnetic subunit. More electronic transport properties and magnetic data are needed to better understand the origin of the ferromagnetism and antiferromagnetism in this material.

4 Conclusions

In this study, we have reported on the synthesis and structural characterization of three new compounds, isostructural, but not isoelectronic with the thermoelectric material $Yb_{14}MnSb_{11}$. They are $Eu_{14}CdAs_{11}$, $Sr_{14}Cd_{1.06(1)}As_{11}$, and $Eu_{14}Cd_{1.27(1)}Sb_{11}$. The structure of $Sr_{14}Cd_{1.30(1)}Sb_{11}$ could be considered as a re-assessment of the previously reported $Sr_{14}CdSb_{11.37}$.[12] Both antimonides display a conspicuous feature of this structure—the presence of additional interstitial Cd atoms. The corresponding arsenides show lesser tendency to be stabilized interstitially, and their structures show the signatures of positional disorder on at least one of the As sites. By judiciously choosing the counter-cations (Eu and Sr) and the two pnictogen atoms (As and Sb), we showed using the Voronoi cell volume that the ''free volume'' is greater in the antimonides than in the corresponding arsenide counterparts. In turn, the greater available space can be correlated with the higher fraction of Cd atoms filling that site. The robust cation–cation bonds observed in the structure might be a natural response of the electronic structure to compensate for the apparent electron deficiency and in order to optimize the bonding interactions. The electronic structure calculations for $Sr_{14}CdSb_{11}$ showed that the Fermi level falls near the edge of the valence band, which agrees well with the metallic-like conductivity. The thermoelectric properties of the air stable compounds warrant to be investigated since the additional interstitial metal atoms could regulate efficiently both the electronic and thermal transport properties.

Acknowledgements

Svilen Bobev acknowledges financial support from the US DOE (Basic Energy Sciences) through a grant DE-SC0008885. The authors are indebted to Dr. N.-T. Suen for his help with the electronic structure calculations.

Notes and references

1 (*a*) S. M. Kauzlarich, in *Chemistry, Structure, and Bonding of Zintl Phases and Ions*, ed. S. M. Kauzlarich, VCH Publishers, New York, 1996, p. 245; (*b*) J. Y. Chan, M. M. Olmstead, S. M. Kauzlarich and D. J. Webb, *Chem. Mater.*, 1998, **10**, 3583; (*c*) J. Y. Chan, M. E. Wang, A. Rehr and S. M. Kauzlarich, *Chem. Mater.*, 1997, **9**, 2131; (*d*) J. Y. Chan, S. M. Kauzlarich, P. Klavins, R. N. Shelton and D. J. Webb, *Chem. Mater.*, 1997, **9**, 3132; (*e*) J. Y. Chan, S. M. Kauzlarich, P. Klavins, R. N. Shelton and D. J. Webb, *Phys. Rev. B: Condens. Matter Mater. Phys.*, 1998, **57**, 8103; (*f*) I. R. Fisher, S. L. Bud'ko, C. Song, P. C. Canfield, T. C. Ozawa and S. M. Kauzlarich, *Phys. Rev. Lett.*, 2000, **85**, 1120; (*g*) R. F. Gallup, C. Y. Fong and S. M. Kauzlarich, *Inorg. Chem.*, 1992, **31**, 115.

2 G. Cordier, H. Schäfer and M. Stelter, *Z. Anorg. Allg. Chem.*, 1984, **519**, 183.

3 (*a*) E. Zintl, *Angew. Chem.*, 1939, **52**, 1; (*b*) H. Schäfer, B. Eisenmann and W. Müller, *Angew. Chem., Int. Ed. Engl.*, 1973, **12**, 694; (*c*) H. Schäfer and B. Eisenmann, *Rev. Inorg. Chem.*, 1981, **3**, 29, and references cited therein.

4 J. T. Vaughey and J. D. Corbett, *Chem. Mater.*, 1996, **8**, 671.

5 A. Rehr, T. Y. Kuromoto, J. DelCastillo, D. J. Webb and S. M. Kauzlarich, *Chem. Mater.*, 1994, **6**, 93.

6 S. M. Kauzlarich and T. Y. Kuromoto, *Croat. Chem. Acta*, 1991, **64**, 343.

7 M. L. Munzarová and R. Hoffmann, *J. Am. Chem. Soc.*, 2002, **124**, 4787.

8 S. M. Kauzlarich, M. M. Thomas, D. A. Odink and M. M. Olmstead, *J. Am. Chem. Soc.*, 1991, **113**, 7205.

9 A. Rehr and S. M. Kauzlarich, *J. Alloys Compd.*, 1994, **207**, 424.

10 T. Y. Kuromoto, S. M. Kauzlarich and D. J. Webb, *Chem. Mater.*, 1992, **4**, 435.

11 Y. Hu, J. Wang, A. Kawamura, K. Kovnir and S. M. Kauzlarich, *Chem. Mater.*, 2015, **27**, 343.

12 D. M. Young, C. C. Torardi, M. M. Olmstead and S. M. Kauzlarich, *Chem. Mater.*, 1995, **7**, 93.

13 S. Q. Xia and S. Bobev, *J. Am. Chem. Soc.*, 2007, **129**, 4049.

14 S. Q. Xia and S. Bobev, *Inorg. Chem.*, 2006, **45**, 7126.

15 S. Q. Xia and S. Bobev, *Chem. – Asian J.*, 2007, **2**, 619.

16 S. Q. Xia and S. Bobev, *J. Comput. Chem.*, 2008, **29**, 2125.

17 S. Q. Xia and S. Bobev, *Inorg. Chem.*, 2008, **47**, 1919.

18 S. Q. Xia and S. Bobev, *J. Am. Chem. Soc.*, 2007, **129**, 10011.

19 (*a*) S. K. Bux, A. Zevalkink, O. Janka, D. Uhl, S. Kauzlarich, J. G. Snyder and J.-P. Fleurial, *J. Mater. Chem. A*, 2014, **2**, 215; (*b*) S. Ohno, A. Zevalkink, Y. Takagiwa, S. K. Bux and G. J. Snyder, *J. Mater. Chem. A*, 2014, **2**, 7478.

20 D. Wilson, B. Saparov and S. Bobev, *Z. Anorg. Allg. Chem.*, 2011, **637**, 2018.

21 *SMART*, Bruker AXS Inc., Madison, Wisconsin, USA, 2003.

22 *SAINT*, Bruker AXS Inc., Madison, Wisconsin, USA, 2003.

23 *SADABS*, Bruker AXS Inc., Madison, Wisconsin, USA, 2003.

24 *SHEXLTL*, Bruker AXS Inc., Madison, Wisconsin, USA, 2003.

25 (*a*) A. Altomare, G. Cascarano, C. Giacovazzo, A. Guagliardi, M. C. Burla, G. Polidori and M. Camalli, *J. Appl. Crystallogr.*, 1994, **27**, 435; (*b*) G. M. Sheldrick, *Acta Crystallogr.*, 2008, **A64**, 112.

26 L. J. Farrugia, *J. Appl. Crystallogr.*, 1999, **32**, 837.

27 L. M. Gelato and E. Parthe, *J. Appl. Crystallogr.*, 1987, **20**, 139.

28 (*a*) O. K. Andersen, *Phys. Rev. B: Solid State*, 1975, **12**, 3060–3083; (*b*) O. K. Andersen and O. Jepsen, *Phys. Rev. Lett.*, 1984, **53**, 2571–2574; (*c*) O. K. Andersen, Z. Pawlowska and O. Jepsen, *Phys. Rev. B: Condens. Matter Mater. Phys.*, 1986, **34**, 5253; (*d*) H. L. Skriver, *The LMTO Method*, Springer, Berlin, 1984.

29 O. Jepsen and O. K. Andersen, *The Stuttgart TB-LMTO Program, Version 4.7*, Max-Planck-Institut für Festkörperforschung, Stuttgart, Germany, 1998.

30 O. K. Andersen, O. Jepsen and D. Glötzel, in *Highlights of Condensed Matter Theory*, ed. F. Bassani, F. Fumi and M. Tosi, North-Holland, New York, 1985.

31 U. von Barth and L. Hedin, *J. Phys. C: Solid State Phys.*, 1972, **5**, 1629.

32 D. D. Koelling and B. N. Harmon, *J. Phys. C: Solid State Phys.*, 1977, **10**, 3107.
33 W. R. L. Lambrecht and O. K. Andersen, *Phys. Rev. B: Condens. Matter Mater. Phys.*, 1986, **34**, 2439.
34 R. Dronskowski and P. E. Blöchl, *J. Phys. Chem.*, 1993, **97**, 8617.
35 P. E. Blöchl, O. Jepsen and O. K. Andersen, *Phys. Rev. B: Condens. Matter Mater. Phys.*, 1994, **49**, 16223.
36 *Pearson's Handbook of Crystallographic Data for Intermetallic Phases*, ed. P. Villars and L. D. Calvert, American Society for Metals, Materials Park, OH, 2nd edn, 1991.
37 A. C. Payne, M. M. Olmstead, S. M. Kauzlarich and D. J. Webb, *Chem. Mater.*, 2001, **13**, 1398.
38 (*a*) L. Pauling, *The Nature of the Chemical Bond*, Cornell University Press, Ithaca, NY, 3rd edn, 1960; (*b*) L. Pauling, *J. Am. Chem. Soc.*, 1929, **51**, 1010.
39 B. Saparov, H. He, X. Zhang, R. Greene and S. Bobev, *Dalton Trans.*, 2010, **39**, 1063.
40 J. P. A. Makongo, T.-S. You, H. He, N.-T. Suen and S. Bobev, *Eur. J. Inorg. Chem.*, 2014, 5113.
41 J. P. A. Makongo, Yu. Prots, R. Niewa, U. Burkhardt and G. Kreiner, *Z. Kristallogr. - New Cryst. Struct.*, 2005, **220**, 291.
42 P. Duwez and J. L. Taylor, *AIME Trans.*, 1950, **188**, 1173.
43 M. V. Nevitt, Miscellaneous Structures of Fixed Stoichiometry, in *Intermetallic Compounds*, ed. J. H. Westbrook, Wiley, New York, 1967, pp. 217–299.
44 R. E. Marsh, *Acta Crystallogr.*, 1954, **7**, 379.
45 J. K. Brandon, R. Y. Brizard, W. B. Pearson and D. J. N. Tozer, *Acta Crystallogr.*, 1977, **B33**, 527.
46 P. Pearce, *Structure in Nature is a Strategy for Design*, MIT Press, Cambridge, 1990.
47 E. A. Lord and S. Ranganathan, *J. Non-Cryst. Solids*, 2004, **334 & 335**, 121.
48 G. Kreiner and M. Schäpers, *J. Alloys Compd.*, 1997, **259**, 83.
49 G. Kreiner and H. F. Franzen, *J. Alloys Compd.*, 1995, **221**, 15.
50 S. Thimmaiah and G. J. Miller, *Chem. – Eur. J.*, 2010, **16**, 5461.
51 S. Bobev, D. J. Thompson, J. L. Sarrao, M. M. Olmstead, H. Hope and S. M. Kauzlarich, *Inorg. Chem.*, 2004, **43**, 5044.
52 S. Q. Xia and S. Bobev, *Chem. Mater.*, 2010, **22**, 840.
53 X.-C. Liu, Z. Wu, S. Q. Xia, X. T. Tao and S. Bobev, *Inorg. Chem.*, 2015, **54**, 947.
54 N. Kazem, A. Hurtado, B. Klobes, R. P. Hermann and S. M. Kauzlarich, *Inorg. Chem.*, 2015, **54**, 850.
55 G. F. Voronoi, *J. Reine Angew. Math.*, 1908, **134**, 198.
56 (*a*) C. Chothia, *Nature*, 1974, **248**, 338; (*b*) F. M. Richards, *Annu. Rev. Biophys. Bioeng.*, 1977, **6**, 151; (*c*) Y. Harpaz, M. Gerstein and C. Chothia, *Structure*, 1994, **2**, 641; (*d*) J. Janin and C. Chothia, *J. Biol. Chem.*, 1990, **265**, 16027; (*e*) F. M. Richards, *Carlsberg Res. Commun.*, 1979, **44**, 47; (*f*) F. M. Richards, *Methods Enzymol.*, 1985, **115**, 440; (*g*) M. Gerstein, A. M. Lesk, E. N. Baker, B. Anderson, G. Norris and C. Chothia, *J. Mol. Biol.*, 1993, **234**, 357; (*h*) J. L. Finney, *J. Mol. Biol.*, 1975, **96**, 721; (*i*) J. L. Finney, B. J. Gellatly, I. C. Golton and J. Goodfellow, *Biophys. J.*, 1980, **32**, 17; (*j*) S. J. Hubbard and P. Argos, *Curr. Opin. Biotechnol.*, 1995, **6**, 375.
57 T. Ringler, L. Ju and M. Gunzburger, *Ocean Dynamics*, 2008, **58**, 475.
58 (*a*) C. H. Rycroft, *Chaos*, 2009, **19**, 041111; (*b*) C. H. Rycrof, Z. Martin, M. Z. Bazant, G. S. Grest and J. W. Landry, *Phys. Rev. E: Stat., Nonlinear, Soft Matter Phys.*, 2006, **73**, 051306; (*c*) K. Kamrin, C. H. Rycroft and M. Z. Bazant, *Modell. Simul. Mater. Sci. Eng.*, 2007, **15**, S449; (*d*) J. P. Shih, S. Y. Sheu and C. Y. Mou, *J. Chem. Phys.*, 1994, **100**, 2202; (*e*) M. Gerstein, J. Tsai and M. Levitt, *J. Mol. Biol.*, 1995, **249**, 955.
59 (*a*) R. Berthold, M. Mihalkovic, U. Burkhardt, Y. Prots, A. Amarsanaa and G. Kreiner, *Intermetallics*, 2014, **53**, 67; (*b*) R. Berthold, G. Kreiner, U. Burkhardt, S. Hoffmann, G. Auffermann, Y. Prots, E. Dashjav, A. Amarsanaa and M. Mihalkovic, *Intermetallics*, 2013, **32**, 259.
60 E. J. Gabe, Y. le Page, P.-P. Charland, F. L. Lee and P. S. White, *J. Appl. Crystallogr.*, 1989, **22**, 384.
61 R. D. Shannon and C. T. Prewitt, *Acta Crystallogr., Sect. B: Struct. Crystallogr. Cryst. Chem.*, 1969, **25**, 925.
62 J. P. A. Makongo, N. T. Suen, S. P. Guo, S. Saha, R. Greene, J. P. Paglione and S. Bobev, *J. Solid State Chem.*, 2014, **211**, 95.

